ISME

Crack Analysis of an Orthotropic Circular Bars Reinforced by a Magnetic Coating under Saint-Venant Torsion

R. Bagheri[*]
Assistant Professor

A. R. Hassani[†]
Ph.D

This paper presents an analytical solution for an orthotropic circular cross section bar with a magnetic coating weakened by multiple arbitrary oriented cracks under Saint-Venant torsion by means of the distributed dislocation technique. At first, the solution of the orthotropic bar with a magnetic coating weakened by a Volterra-type screw dislocation is achieved with the aid of the finite Fourier sine transform. Next, the problem is then reduced to a set of singular integral equations with a Cauchy type singularity. Unknown dislocation density is achieved by numerical solution of these integral equations. Finally, several examples are solved and numerical results are discussed to reveal the effect of the magnetic layer on the reduction of the mechanical stress intensity factor in the bar.

Keywords: Saint-Venant torsion, Orthotropic circular bar, Magnetic coating, Stress intensity factor, Multiple cracks

1 Introduction

Application of smart materials and structures has been grown recently. Sensors and actuators are examples of active components made of smart materials which were used widely in smart structures. These components are widely subjected to mechanical loading. Specially, the torsion analysis of those is of special interest. The torsion problem of intact bars or beams made of smart materials was treated by a few researchers [1-6]. Whereas the torsion problem of cracked smart bars or cracked isotropic bars with smart material coating was not considered by other investigators. Because of the lack of such studies, the review is only allocated to the articles relating to intact bars or beams under torsion. Ecsedi and Baksa [1, 2] presented a direct and a variational formulation for the torsional problem of elastoelectric beams or homogeneous, linear piezoelectric monoclinic beams. It has been done by a generalization of the Saint-Venant's torsion theory of elastic beams to piezoelastic beams. The problem was formulated in terms of Prandtl's stress function and electric displacement potential function which construct the coupled Dirichlet problem in the cross-sectional domain. As the case studies, the torsional problem of thin-walled piezoelastic beams with closed cross-section such as rectangular box, and the torsion of hollow circular cylinders made of orthotropic piezoelectric material were investigated [1].

[*] Corresponding Author, Assistant Professor, Department of Mechanical Engineering, Karaj Branch, Islamic Azad University, Karaj, Iran r.bagheri@kiau.ac.ir

[†] Ph.D, Department of Mechanical Engineering, Karaj Branch, Islamic Azad University, Karaj, Iran a.hassani1111@gmail.com

Receive : 2018/12/20 Accepted : 2019/07/14

Also, exact solutions for solid elliptical and hollow circular cross-sections were presented [2]. The analytical formulations were given for torsion problem of monoclinic piezoelectric hollow bars with uniform thickness by Talebanpour and Hematiyan [3]. The cross-section was composed of some straight and curved segments. Similar to references [1, 2] the governing equations were based on Prandtl's stress and electric displacement potential functions. A variational method was used to analyze the problem. Some examples including the piezoelectric rounded square, flattened and rounded triangular tubes were studied. Using the theory of elasticity, exact analytical and numerical solutions for static torsion problem of a piezoelectric rod were found by Maleki et al. [4]. The range of valid region for assumption of linear distribution of electric potential through the cross section and shape-effects on induced piezoelectric deformation were studied. In other study, Maleki et al. [5] presented the exact solution for torsion of multilayer piezoelectric bars with rectangular cross section. In this new study, multilayer piezoelectric materials with different properties were considered while the axis of torsion and the polarization axes of each layer make different orientations with respect to each other. Zehetner [6] investigated the compensation of the angle of twist caused by external torsional moments in rods based on the Saint-Venant's theory of uniform torsion. It was accomplished by use of the thin integrated piezoelectric actuator layers. To this end, a laminated orthotropic rod with homogenous layers was considered. This compensation was done by distributing of the piezoelectric strains or Eigen-strains. An analytic solution for the actuating moment in an example of a rectangular cross section was given.

In the present work torsion analysis of a cracked isotropic bar subjected to torsion is studied. An outer magneto-elastic coating layer was employed as an actuator which the bar and its coating are under both mechanical and magnetic loading. The loadings are including a torsional torque around the bar axis and a magnetic induction on the outer surface of the coating layer. The cracks are only in the isotropic bar. The main scope of the present paper is to find a proper value of a non-dimensional parameter presenting the effect of magnetic loading and the coating thickness on the stress intensity factor of the crack tip. The magneto-elastic actuation is used in order to completely compensate the torsion due to external torque and remove the mechanical stress intensity factor on the crack tips. According to the above review, the torsion problem of the cracked bars of circular cross-section with a magneto-elastic coating is an interesting problem. The previous studies were limited only to torsion of the intact bars. To the authors' knowledge, no solution has been reported yet on the torsion compensation analysis of a cracked bar of circular cross-section with the multiple arbitrary oriented curved cracks. In the sections to follow, the analytical solution to stress field is first carried out for an isotropic coated bar with a circular cross-section weakened by one screw dislocation. The bar was under both torsion and the actuation of a magneto-elastic coating layer (Section 2.1). Formula for evaluation of the torsional rigidity of the cracked circular bars is presented (Section 2.2). Section 3 presents the distributed dislocation for these solutions to formulate and solve the Cauchy-type singular integral equations for the domain weakened by several axisymmetric cracks. The numerical examples will be presented to validate the results of the paper and to understand the effect of the problem parameters on the ensuing stress intensity factors at the crack tips (Section 4). Finally, section 5 offers concluding remarks.

2 Problem formulation

2.1 Dislocation solution

Consider an isotropic circular bar with a magnetic coating as shown in Fig. (1). The circular cylindrical coordinate selected such that the z-axis is along the longitudinal direction and the origin is located at the center of the cross-section.

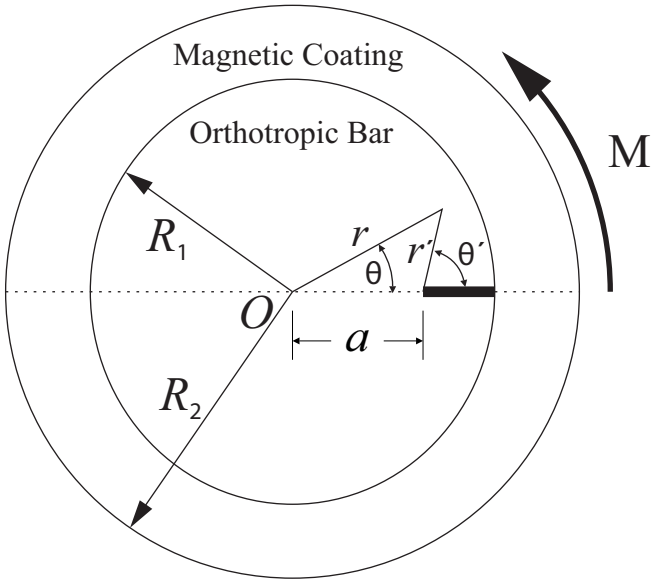

Figure 1 Circular cross-section of a bar with a magnetic coating containing a screw dislocation

In Fig. (1), R_1 is the radius of the circular shaft and the thickness of the coating is assumed to be $R_2 - R_1$. A screw dislocation, which has a Burgers vector whose magnitude is b_z, is situated at $r = a$ which the dislocation cut is a radial outward cut on the line of $\theta = 0, a \leq r \leq R_1$. As such, the cross-section consists of three regions, $r \leq a$, $a \leq r \leq R_1$ and $R_1 \leq r \leq R_2$, which are attached together along the circles $r = a$ and $r = R_1$, respectively.
With the aid of the analytical solution of the generalized Saint–Venant's torsion theorem, [2] we have

$$\begin{aligned} u &= -\alpha yz \\ v &= \alpha xz \\ w &= \alpha\omega(x,y) \\ \varphi &= \alpha\phi(x,y) \end{aligned} \tag{1}$$

In which, u, v and w are the displacement components in x, y and z directions, respectively, α is the angle of twist per unit length of the bar, $\omega(x,y)$ is the torsional warping function and $\varphi(x,y)$ is the magnetic potential function. Eqs. (1) are valid in the whole domain (both of bar and its coating) with same value of α, but the magnetic potential function is the zero in the bar. By transformation of the cylindrical coordinates to the Cartesian coordinates, Eqs (1) can be rewritten as

$$u_r = 0, u_\theta = \alpha rz, w = \alpha\omega(r,\theta), \varphi = \alpha\phi(r,\theta) \tag{2}$$

First, we analyze the domain, specifying the bar cross section, i.e. the regions 1 and 2.
The nonzero strains are only two shear strains, that is, ε_{rz} and $\varepsilon_{\theta z}$, which those strains are related to the warping function as

$$\begin{aligned} \varepsilon_{rz} &= \frac{1}{G_{rz}}\tau_{rz} = \alpha\frac{\partial\omega(r,\theta)}{\partial r} \\ \varepsilon_{\theta z} &= \frac{1}{G_{\theta z}}\tau_{\theta z} = \alpha\left(\frac{1}{r}\frac{\partial\omega(r,\theta)}{\partial\theta} + r\right) \end{aligned} \tag{3}$$

where $G_{rz}, G_{\theta z}$ are the shear modulus of the orthotropic bar. After calculating corresponding stress field and substituting the result into the equilibrium equation $\frac{\partial}{\partial r}(r\tau_{rz}) + \frac{\partial\tau_{\theta z}}{\partial\theta} = 0$, in the absence of body forces, a governing equation in terms of $\omega(r,\theta)$ is obtained:

$$r^2\frac{\partial^2\omega(r,\theta)}{\partial r^2} + r\frac{\partial\omega(r,\theta)}{\partial r} + G^2\frac{\partial^2\omega(r,\theta)}{\partial\theta^2} = 0 \tag{4}$$

here $G = \sqrt{G_{\theta z}/G_{rz}}$ is defined as the orthotropic ratio in the coating.. It is necessary to use the finite Fourier sine transform with respect to the variable θ, that is

$$F_s(n) = \int_0^{\pi} f(\theta)\, sin(n\theta)\, d\theta \tag{5}$$

The inverse of the finite Fourier sine transform is expressed by

$$f(\theta) = \frac{2}{\pi}\sum_{n=1}^{\infty} F_s(n)\, sin(n\theta) \tag{6}$$

It is also important to mention that the torque M is first applied on the bar with its coating and then the dislocation cut is made. Therefore, the generalized Saint–Venant's torsion theorem, i.e., Eqs. (1) is valid to solve the dislocation problem.

Boundary and continuity conditions of dislocation cut in the bar may be stated as follows

$$\begin{gathered}\omega(r,0^+) - \omega(r,0^-) = \frac{b_z}{\alpha}[H(r-a) - H(r-R_1)] \\ \frac{\partial\omega(r,0^+)}{\partial\theta} = \frac{\partial\omega(r,0^-)}{\partial\theta}\end{gathered} \tag{7}$$

where $H(.)$ is the Heaviside step function. It is worth mentioning that the first condition of (7) is a jump condition in displacement and the second one is the condition for continuity of the stress component $\tau_{\theta z}$ on the dislocation cut. Because the problem is anti-symmetric with respect to the diameter of domain, $\theta = 0$, we can consider the dislocation solution for the region $0 \le \theta \le \pi$ as

$$\begin{gathered}\omega(r,0^+) = \frac{b_z}{2\alpha}[H(r-a) - H(r-R_1)] \\ \omega(r,\pi) = 0\end{gathered} \tag{8}$$

Applying the integral transform (5) to Eq. (4) yields

$$r^2\frac{\partial^2\bar{\omega}}{\partial r^2} + r\frac{\partial\bar{\omega}}{\partial r} - G^2n^2\bar{\omega}(r,n) = -n\frac{b_z}{2\alpha}[H(r-a) - H(r-R_1)] \tag{9}$$

Solution of the last differential equation (9), in the regions 1 and 2, can be put in the form

$$\begin{gathered}\omega(r,\theta) = \frac{2}{\pi}\sum_{n=1}^{\infty} A_{1n}r^{nG}sin(n\theta)\,, \qquad 0 \le r \le a \\ \omega = \frac{2}{\pi}\sum_{n=1}^{\infty}(A_{2n}r^{Gn} + B_{2n}r^{-Gn} + \frac{b_z}{2n\alpha})sin(n\theta)\,,\ a \le r \le R_1\end{gathered} \tag{10}$$

The solution of the problem can also be represented in the form of exponential functions but in order to easy compare the resulting stress field in the special case i.e. $G = 1$ with those in the literature we state the solution in the presented form. Now, we try to find stress field in the magnetic layer. In the region 3, The constitutive equation in the polar coordinates is given as [11]

$$\begin{bmatrix}\tau_{\theta z}\\ \tau_{rz}\\ B_\theta\\ B_r\end{bmatrix} = \begin{bmatrix}C_{44} & 0 & -h_{15} & 0\\ 0 & C_{44} & 0 & -h_{15}\\ h_{15} & 0 & \gamma_{11} & 0\\ 0 & h_{15} & 0 & \gamma_{11}\end{bmatrix}\begin{bmatrix}\varepsilon_{\theta z}\\ \varepsilon_{rz}\\ H_\theta\\ H_r\end{bmatrix} \tag{11}$$

where $\tau_{\theta z}, \tau_{rz}$ and $\varepsilon_{\theta z}, \varepsilon_{rz}$ are the mechanical shear stresses and strains, respectively. B_r, B_θ are the magnetic inductions and H_r, H_θ are the magnetic fields. Also C_{44} is the elastic shear stiffness constant of the magnetic coating, h_{15} and γ_{11} are the piezomagnetic coefficient and magnetic permeability, respectively. The magnetic field components can be expressed in terms of an magnetic potential $\varphi(r,\theta)$, as

$$\begin{gathered}H_r = -\frac{\partial\varphi}{\partial r} = -\alpha\frac{\partial\phi}{\partial r} \\ H_\theta = -\frac{1}{r}\frac{\partial\varphi}{\partial\theta} = -\frac{\alpha}{r}\frac{\partial\phi}{\partial\theta}\end{gathered} \tag{12}$$

The nonzero mechanical strain can be calculated with help of Eq. (3) equilibrium equations for the stresses and the magnetic inductions are

$$\frac{\partial}{\partial r}(r\tau_{rz}) + \frac{\partial \tau_{\theta z}}{\partial \theta} = 0$$
$$\frac{\partial}{\partial r}(rB_r) + \frac{\partial B_\theta}{\partial \theta} = 0 \tag{13}$$

Upon substituting Eqs. (3) and (12) into above equations and substituting the ensuing equations into Eqs. (13), we arrive at

$$C_{44}\nabla^2\omega + h_{15}\nabla^2\phi = 0$$
$$h_{15}\nabla^2\omega - \gamma_{11}\nabla^2\phi = 0 \tag{14}$$

Since the determinant of the matrix $\begin{pmatrix} C_{44} & h_{15} \\ h_{15} & -\gamma_{11} \end{pmatrix}$ is the nonzero number, the condition for the existence of nontrivial solutions for the above equations in terms of variables $\nabla^2\omega$ and $\nabla^2\phi$ implies that

$$\nabla^2\omega = 0$$
$$\nabla^2\phi = 0 \tag{15}$$

The solution to the equations $\nabla^2\omega = 0$, is similar to that of given in the second equation of (10) but with different coefficients, that is

$$\omega(r,\theta) = \frac{2}{\pi}\sum_{n=1}^{\infty}(A_{3n}r^n + B_{3n}r^{-n})sin(n\theta)\,, R_1 \le r \le R_2 \tag{16}$$

We also propose the similar solution form to equation $\nabla^2\phi = 0$ as follows

$$\phi(r,\theta) = \frac{2}{\pi}\sum_{n=1}^{\infty}(C_n r^n + D_n r^{-n})sin(n\theta)\,, R_1 \le r \le R_2 \tag{17}$$

The unknown coefficient of Eqs. (10), (16) and (17) must be determined by following boundary and continuity conditions

$$\omega(a^-,\theta) = \omega(a^+,\theta)$$
$$\tau_{rz}(a^-,\theta) = \tau_{rz}(a^+,\theta)$$
$$\tau_{rz}(R_2,\theta) = 0$$
$$B_r\,(R_2,z) = B_0$$
$$B_r\,(R_1,z) = 0$$
$$\tau_{rz}(R_1^-,\theta) = \tau_{rz}(R_1^+,\theta)$$
$$\omega(R_1^-,\theta) = \omega(R_1^+,\theta) \tag{18}$$

where B_0 is magnetic induction in the outer radii of the magnetic layer. As we will explain in the following, the magnetic layer will play role of an actuator and thus its outer radii can be imposed to the magnetic induction. Required coefficients are solved to yield

$$A_{1n} = a^{-n}\Gamma_n\{\frac{b_z}{4n\alpha}[2(\rho_n\kappa_n^2 - \rho_n) + (C_{eq} - 1)(\kappa_n^2 - \rho_n^2) + (1 + C_{eq})(1 - \rho_n^2\kappa_n^2)]$$
$$+2B_0R_2\kappa_n\frac{h_{15}C_{eq}}{G\gamma_{11}}\rho_n\frac{1-(-1)^n}{n^2\alpha}\}$$
$$A_{2n} = R_1^{-n}\Gamma_n\{-\frac{b_z}{4n\alpha}[2 + (C_{eq} - 1)\rho_n - 2\kappa_n^2 + (C_{eq} + 1)\rho_n\kappa_n^2]$$
$$+2B_0R_2\kappa_n\frac{h_{15}C_{eq}}{G\gamma_{11}}\frac{1-(-1)^n}{n^2\alpha}\}$$
$$B_{2n} = -\frac{b_z}{4n\alpha}a^n \tag{19}$$

in which

$$\kappa_n = (\frac{R_1}{R_2})^n$$
$$\rho_n = (\frac{a}{R_1})^n$$

$$C_{eq}=\frac{G\gamma_{11}G_{rz}}{h_{15}^2+\gamma_{11}C_{44}}$$
$$\Gamma_n=(\frac{1}{C_{eq}+1})\frac{1}{1-\eta\kappa_n^2} \tag{20}$$

wherein $\eta=\frac{1-C_{eq}}{1+C_{eq}}$. We did not bring the coefficients A_{3n}, B_{3n}, C_n and D_n here because in this article we assume that the cracks to be only in the isotropic bar not in the coting. Therefore, the stress field inside the coating will not use directly and the related coefficients are given in appendix A. Substituting the coefficients (19) into Eqs. (10) and inserting the ensuing equations into Eqs. (3), the shear stress components for the bar are given by

$$\tau_{rz}=\frac{2G\alpha}{\pi r}\sum_{n=1}^{\infty}n(\frac{r}{a})^n\Gamma_n\{\frac{b_z}{4n\alpha}[2(\rho_n\kappa_n^2-\rho_n)+\big(C_{eq}-1\big)(\kappa_n^2-\rho_n^2)+(1+C_{eq})$$
$$(1-\rho_n^2\kappa_n^2)]+2B_0R_2\kappa_n\rho_n\frac{1-(-1)^n}{n^2\alpha}\frac{h_{15}C_{eq}}{G\gamma_{11}}\}sin(n\theta)$$
$$,0\le r\le a$$
$$\tau_{rz}=\frac{2G\alpha}{\pi r}\sum_{n=1}^{\infty}n\{\Gamma_n\{-\frac{b_z}{4n\alpha}[2+(C_{eq}-1)\rho_n-2\kappa_n^2+(C_{eq}+1)\rho_n\kappa_n^2]$$
$$+2B_0R_2\kappa_n\frac{1-(-1)^n}{n^2\alpha}\frac{h_{15}C_{eq}}{G\gamma_{11}}\}(\frac{r}{R_1})^n$$
$$+\frac{b_z}{4n\alpha}(\frac{a}{r})^n\}sin(n\theta),a\le r\le R_1$$
$$\tau_{\theta z}=\frac{2G\alpha}{\pi r}\sum_{n=1}^{\infty}n(\frac{r}{a})^n\Gamma_n\{\frac{b_z}{4n\alpha}[2(\rho_n\kappa_n^2-\rho_n)+\big(C_{eq}-1\big)(\kappa_n^2-\rho_n^2)+(1+C_{eq})$$
$$(1-\rho_n^2\kappa_n^2)]+2B_0R_2\kappa_n\rho_n\frac{1-(-1)^n}{n^2\alpha}\frac{h_{15}C_{eq}}{G\gamma_{11}}\}cos(n\theta)$$
$$+rG\alpha,\quad 0\le r\le a$$
$$\tau_{\theta z}=-\frac{b_zG}{2\pi r}+\frac{2G\alpha}{\pi r}\sum_{n=1}^{\infty}n\{\Gamma_n\{-\frac{b_z}{4n\alpha}[2+(C_{eq}-1)\rho_n-2\kappa_n^2+(C_{eq}+1)\rho_n\kappa_n^2]$$
$$+2B_0R_2\kappa_n\frac{1-(-1)^n}{n^2\alpha}\frac{h_{15}C_{eq}}{G\gamma_{11}}\}(\frac{r}{R_1})^n$$
$$-\frac{b_z}{4n\alpha}(\frac{a}{r})^n\}cos(n\theta)+rG\alpha,\qquad a\le r\le R_1 \tag{21}$$

Knowing $\eta\kappa_n^2<1$, we write a MacLaurin expansion for Γ_n, in the following form

$$\Gamma_n=\frac{1}{C_{eq}+1}\sum_{m=0}^{\infty}\eta^m{\kappa_n}^{2m} \tag{22}$$

Using Eq. (22) and doing some manipulations, Eqs. (21) are rewritten in the term of four new functions E_m, F_m, G_m and H_m as follows

$$\tau_{rz}=\frac{2h_{15}C_{eq}}{\pi r\gamma_{11}\big(C_{eq}+1\big)}\Psi(r,\theta)+\frac{G_{rz}b_z}{4\pi r}\frac{1}{1+C_{eq}}\sum_{m=0}^{\infty}\eta^m[2(E_m(\frac{rR_1}{R_2^2},\theta)$$
$$-E_m(\frac{r}{R_1},\theta))+\big(C_{eq}-1\big)(E_m(\frac{rR_1^2}{aR_2^2},\theta)-E_m(\frac{ar}{R_1^2},\theta))$$
$$+(1+C_{eq})(E_m(\frac{r}{a},\theta)-E_m(\frac{ar}{R_2^2},\theta))],0\le r\le a$$
$$\tau_{rz}=\frac{2h_{15}C_{eq}}{\pi r\gamma_{11}(C_{eq}+1)}\Psi(r,\theta)+\frac{G_{rz}b_z}{4\pi r}\frac{1}{C_{eq}+1}\{(C_{eq}+1)E_0(\frac{a}{r},\theta)-\sum_{m=0}^{\infty}\eta^m$$

$$[2E_m(\frac{r}{R_1},\theta)+(C_{eq}-1)E_m(\frac{ar}{R_1^2},\theta)-2E_m(\frac{R_1 r}{R_2^2},\theta)+(C_{eq}+1)E_m(\frac{ar}{R_2^2},\theta)]\}$$
$$,a\le r\le R_1$$
$$\tau_{\theta z}=\frac{2h_{15}C_{eq}}{\pi r\gamma_{11}(C_{eq}+1)}\Phi(r,\theta)$$
$$+\frac{G_{\theta z}b_z}{4\pi r}\frac{1}{C_{eq}+1}\{\sum_{m=0}^{\infty}\eta^m[2(F_m(\frac{r}{R_1},\theta)-F_m(\frac{R_1 r}{R_2^2},\theta))$$
$$+\big(C_{eq}-1\big)(F_m(\frac{ar}{R_1^2},\theta)-F_m(\frac{R_1^2 r}{R_2^2 a},\theta))+(1+C_{eq})(F_m(\frac{ar}{R_2^2},\theta)-F_m(\frac{r}{a},\theta))]$$
$$+rG\alpha,0\le r\le a$$
$$\tau_{\theta z}=\frac{2h_{15}C_{eq}}{\pi r\gamma_{11}(C_{eq}+1)}\Phi(r,\theta)+\frac{G_{\theta z}b_z}{4\pi r}\frac{1}{C_{eq}+1}\{\big(C_{eq}+1\big)F_0(\frac{a}{r},\theta)-\sum_{m=0}^{\infty}\eta^m$$
$$[2F_m(\frac{R_1 r}{R_2^2},\theta)-2F_m(\frac{r}{R_1},\theta)-(C_{eq}-1)F_m(\frac{ar}{R_1^2},\theta)-(C_{eq}+1)F_m(\frac{ar}{R_2^2},\theta)]\}+rG\alpha$$
$$,a\le r\le R_1 \qquad (23)$$

where

$$\Psi(r,\theta)=2B_0R_2\sum_{m=0}^{\infty}\eta^m\,G_m(\frac{r}{R_2},\theta)$$
$$\Phi(r,\theta)=2B_0R_2\sum_{m=0}^{\infty}\eta^m\,H_m(\frac{r}{R_2},\theta) \qquad (24)$$

and the above-mentioned new functions are introduced as

$$E_m(x,\theta)=2\sum_{n=1}^{\infty}(\kappa_m^2 x)^n sin(n\theta)$$
$$F_m(x,\theta)=-1-2\sum_{n=1}^{\infty}(\kappa_m^2 x)^n cos(n\theta)$$
$$G_m(x,\theta)=\sum_{n=1}^{\infty}\frac{1-(-1)^n}{n}(\kappa_m^2 x)^n sin(n\theta)$$
$$H_m(x,\theta)=\sum_{n=1}^{\infty}\frac{1-(-1)^n}{n}(\kappa_m^2 x)^n cos(n\theta) \qquad (25)$$

With the help of the summation formula given in the appendix of the reference [12] for the series $\sum_{n=1}^{\infty}k^n sin(n\theta)$ and $\sum_{n=1}^{\infty}k^n cos(n\theta),|k|<1$, and also the summation formula extracted from the reference [12] for $\sum_{n=1}^{\infty}\frac{k^{2n-1}}{2N-1}sin((2n-1)\theta)$ and $\sum_{n=1}^{\infty}\frac{k^{2n-1}}{2N-1}cos((2n-1)\theta)$ we arrive at

$$E_m(x,\theta)=\frac{sin\,\theta}{cosh(ln(x\kappa_m^2))-cos\,\theta}$$
$$F_m(x,\theta)=\frac{sinh(ln(x\kappa_m^2))}{cosh(ln(x\kappa_m^2))-cos\,\theta}$$
$$G_m(x,\theta)=\frac{1}{4}tan^{-1}(\frac{2\kappa_m^2 x}{1-\kappa_m^4 x^2}sin\theta)$$
$$H_m(x,\theta)=\frac{1}{4}coth^{-1}(\frac{2\kappa_m^2 x}{1+\kappa_m^4 x^2}sin\theta) \qquad (26)$$

If the coating thickness to be vanished ($B_0=0,R_1=R_2$), the stress fields (23) are simplified as

$$\tau_{rz} = \frac{Gb_z}{4\pi r}[E_0(\frac{r}{a},\theta) - E_0(\frac{ar}{R^2},\theta)],0 \le r \le a$$
$$\tau_{rz} = \frac{Gb_z}{4\pi r}[E_0(\frac{a}{r},\theta) - E_0(\frac{ar}{R^2},\theta)], a \le r \le R$$
$$\tau_{\theta z} = \frac{Gb_z}{4\pi r}[F_0(\frac{ar}{R^2},\theta) - F_0(\frac{r}{a},\theta)] + rG\alpha, 0 \le r \le a$$
$$\tau_{\theta z} = \frac{Gb_z}{4\pi r}[F_0(\frac{ar}{R^2},\theta) + F_0(\frac{a}{r},\theta)] + Gr\alpha, a \le r \le R \quad (27)$$

The above stress field can be validated by reference [8]. There may be two reasons to rewrite stress component (21) in the form of Eqs. (23). First, since the series including pre-defined functions $E_m$and E_m rapidly converge with increasing index m. Also for special case, $B_0 = 0, R_1 = R_2$ (the bar without the coating), the stress components are simplified as the closed form relations.

Also type of the singularity of the stress fields near the dislocation location i.e. $r = a$ is the Cauchy type, namely $1/r'$ where r' is the distance from the dislocation position, Fig. (1). The existence of this kind of singularity has been proved in the reference [8].

For minimization of the mechanical stress intensity factors, we must decrease the resultant external loading on the surfaces of the crack. Therefore, magnetic induction is considered on the outer radius of the coating.

2.2 Torsional rigidity

Considering a torque M applying to the bar, relation between the torsional rigidity J and the shear stress component $\tau_{\theta z}$ takes the following form [13]

$$M = J\alpha = \int_0^{2\pi}\int_0^{R_2} r^2\tau_{\theta z}dr\,d\theta \quad (28)$$

By substituting the Eq. (3) and (11) in the above equation, we get

$$J = J_0 - \frac{1}{2}G(R_1^2 - a^2)\frac{b_z}{\alpha} \quad (29)$$

where

$$J_0 = \frac{1}{2}\pi\left(GR_1^4 + C_{44}(R_2^4 - R_1^4)\right) \quad (30)$$

It is noteworthy that, the torsional rigidity in Eq. (29) has depending on the dislocation density b_z and the torsional rigidity takes the form of Eq. (30) in the intact bar.

3 Analysis with multiple cracks

Now, the dislocation distributed method is employed to analyze the defined problem which is a coated bar weakened by the multiple cracks.

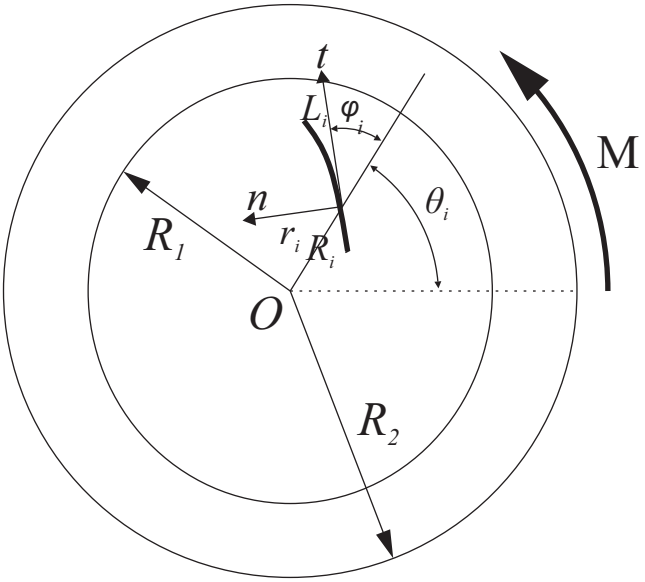

Figure 2 Circular cross-section of the bar with a magnetic coating containing a smooth embedded crack

Herein, we define a local coordinate system $(n-t)$ on each crack to give normal and tangential stress on the crack surfaces.

$$\tau_{tz}(r,\theta) = \tau_{\theta z}(r,\theta)sin\varphi_i + \tau_{rz}(r,\theta)cos\varphi_i$$
$$\tau_{nz}(r,\theta) = \tau_{\theta z}(r,\theta)cos\varphi_i - \tau_{rz}(r,\theta)sin\varphi_i \quad (31)$$

where φ_i is the angle between the tangent to each point of the i-th crack and the radial position vector of that point. We drive the stress field of the bar by use of the distributed dislocation technique. The stress fields also satisfy equilibrium requirements and boundary conditions. For a circular cross-section bar weakened by multiple cracks, governing equation and outer boundary conditions remain unchanged. Only, the surfaces of the cracks should be traction-free. The parameter b_z is a controlling that is set such that the traction-free condition on the surfaces of the cracks to be satisfied.

Now, we distribute the dislocations with unknown density b_z on the infinitesimal segment $d\lambda_j$ situated at the point (r_i,θ_i) of the surface of the j-th crack. The tractions on the surfaces of the cracks are achieved by substituting from Eq. (23) into Eq. (31) .Since the dislocation cut has located at $\theta = 0$, we must replace θ by $\theta_i - \theta_j$ to derive the traction on the surface of the i-th crack. Therefore we arrive at

$$\tau_{nz}(r_i,\theta_i) = \frac{2h_{15}C_{eq}}{\pi\gamma_{11}(C_{eq}+1)r_i}[\Phi(r_i,\theta_i-\theta_j)cos\varphi_i - \Psi(r_i,\theta_i-\theta_j)sin\varphi_i$$
$$+G^2 b_{zj}d\lambda_j \frac{1}{2J_0}\left(R_1^2 - r_j^2\right)r_i\, cos\varphi_i$$
$$+\frac{Gb_{zj}d\lambda_j}{4\pi r_i}\frac{1}{C_{eq}+1}\{\sum_{m=0}^{\infty}\eta^m[2(F_m(\frac{r_i}{R_1},\theta_i-\theta_j) - F_m(\frac{R_1 r_i}{R_2^2},\theta_i-\theta_j))$$
$$+\left(C_{eq}-1\right)(F_m(\frac{r_i r_j}{R_1^2},\theta_i-\theta_j) - F_m(\frac{R_1^2 r_i}{R_2^2 r_j},\theta_i-\theta_j)) + (1+C_{eq})(F_m(\frac{r_i r_j}{R_2^2},\theta_i-\theta_j)$$
$$-F_m(\frac{r_i}{r_j},\theta_i-\theta_j))]cos\varphi_i - \sum_{m=0}^{\infty}\eta^m[2(E_m(\frac{R_1 r_i}{R_2^2},\theta_i-\theta_j)$$

$$-E_m(\frac{r_i}{R_1},\theta_i-\theta_j))+\big(C_{eq}-1\big)(E_m(\frac{R_1^2 r_i}{R_2^2 r_j},\theta_i-\theta_j)-E_m(\frac{r_i r_j}{R_1^2},\theta_i-\theta_j))$$
$$+(1+C_{eq})(E_m(\frac{r_i}{r_j},\theta_i-\theta_j)-E_m(\frac{r_i r_j}{R_2^2},\theta_i-\theta_j))]sin\varphi_i\}+\frac{GM}{J_0}r_i\,cos\varphi_i, 0\le r_i\le r_j$$
$$\tau_{nz}(r_i,\theta_i)=\frac{2h_{15}C_{eq}}{\pi\gamma_{11}\big(C_{eq}+1\big)r_i}[\Phi(r_i,\theta_i-\theta_j)cos\varphi_i-\Psi(r_i,\theta_i-\theta_j)sin\varphi_i]$$
$$+G^2 b_{zj}d\lambda_j\frac{1}{2J_0}\big(R_1^2-r_j^2\big)r_i\,cos\varphi_i$$
$$+\frac{Gb_{zj}d\lambda_j}{4\pi r_i}\frac{1}{C_{eq}+1}\{\big(C_{eq}+1\big)[F_0(\frac{r_j}{r_i},\theta_i-\theta_j)cos\varphi_i-E_0(\frac{r_j}{r_i},\theta_i-\theta_j)sin\varphi_i]$$
$$-\sum_{m=0}^{\infty}\eta^m\,[2F_m(\frac{R_1 r_i}{R_2^2},\theta_i-\theta_j)-2F_m(\frac{r_i}{R_1},\theta_i-\theta_j)$$
$$-(C_{eq}-1)F_m(\frac{r_j r_i}{R_1^2},\theta_i-\theta_j)-(C_{eq}+1)F_m(\frac{r_j r_i}{R_2^2},\theta_i-\theta_j)]cos\varphi_i$$
$$+\sum_{m=0}^{\infty}\eta^m\,[2E_m(\frac{r_i}{R_1},\theta_i-\theta_j)+(C_{eq}-1)E_m(\frac{r_j r_i}{R_1^2},\theta_i-\theta_j)$$
$$-2E_m(\frac{R_1 r_i}{R_2^2},\theta_i-\theta_j)+(C_{eq}+1)E_m(\frac{r_j r_i}{R_2^2},\theta_i-\theta_j)]sin\varphi_i\}+\frac{GM}{J_0}r_i\,cos\varphi_i, r_j\le r_i\le R_1 \tag{32}$$

With regard to $\alpha=M/D$, the above relations are integrated on non-dimensional crack length to find traction on the surface of the crack. Since the crack surface is traction-free, the established integral is zero. If the terms without b_z to be budged to the other side of the equality, an integral equation is established as following form

$$Q_i\big(r_i(s),\theta_i(s)\big)=\sum_{j=1}^{N}\int_{-1}^{1}k_{ij}(s,t)b_{zj}(t)dt\,,\qquad -1\le s\le 1,\qquad i=1,2,\dots,N \tag{33}$$

In which kernels $k_{ij}(s,t)$ and $Q_i\big(r_i(s),\theta_i(s)\big)$ are given in the Appendix B.
The considerations of single-valuedness displacement require that [8]

$$\int_{-1}^{1}\sqrt{[r_j'(t)]^2+[r_j(t)\theta_j'(t)]^2}\,b_{zj}(t)dt=0 \tag{34}$$

where $d\lambda_j=\sqrt{[r_j'(t)]^2+[r_j(t)\theta_j'(t)]^2}dt$ is the infinitesimal segment on the jth crack. The Eqs. (33) and (34) are in terms of dislocations density and must be solved simultaneously. If the crack is an embedded crack, the solution for $b_{zj}(t)$ is of the following form

$$b_{zj}(t)=\frac{g_{zj}(t)}{\sqrt{1-t^2}}\,,\qquad -1\le t\le 1 \tag{35}$$

By distributing a set of dislocation densities along the borders of the cracks and substituting $\alpha=M/J$ as well as viewing the Eq. (30), the torsional rigidity in the cracked bar is achieved as follows

$$J=J_0/[1+\frac{G}{2M}\sum_{j=1}^{N}\int_{-1}^{1}\big(R_1^2-r_j(t)^2\big)\sqrt{[r_j'(t)]^2+[r_j(t)\theta_j'(t)]^2}\,b_{zj}(t)dt] \tag{36}$$

In which N is the number of the cracks. The evaluation of the torsional rigidity can be done by discretizing the integral appeared in Eq. (36) at specific discrete points [8]. The domain of the integral is discretized at m collocation points $t_k = \cos\left(\frac{(2k-1)\pi}{2m}\right)$. Therefore, the torsional rigidity is of the following form

$$J = J_0/[1 + \frac{\pi G}{2Mm}\sum_{j=1}^{N}\sum_{k=1}^{m}\left(R_1^2 - r_j(t)^2\right)\sqrt{[r_j'(t)]^2 + [r_j(t)\theta_j'(t)]^2}\, g_{zj}(t_k)] \tag{37}$$

After evaluating $g_{zj}(t)$, the mechanical stress intensity factors at the crack tips may be defined and obtained as below [8]

$$\mathrm{k_{IIILi}} = \frac{\sqrt{\pi}}{2}\mathrm{G}\left[[\mathrm{r_j'}(-1)]^2 + [\mathrm{r_j}(-1)\theta_\mathrm{j}'(-1)]^2\right]^{\frac{1}{4}}\mathrm{g_{zj}}(-1)$$
$$\mathrm{k_{IIIRi}} = \frac{\sqrt{\pi}}{2}\mathrm{G}\left[[\mathrm{r_j'}(1)]^2 + [\mathrm{r_j}(1)\theta_\mathrm{j}'(1)]^2\right]^{\frac{1}{4}}\mathrm{g_{zj}}(1) \tag{38}$$

4 Numerical Examples

For numerical results, $\lambda = 10^{-10}\frac{h_{15}B_0}{\gamma_{11}C_{44}}$ is the non-dimensional parameter presenting the effect of the magnetic induction loading on the stress intensity factor. Assume that the magnetic layer has the properties as: $C_{44} = 4.5 \times 10^{10}[N/m^2], h_{15} = 550[N/A\,m], \gamma_{11} = 157 \times 10^{-6}[N\,S^2/C^2]$. Also, we have $G_{rz} = 80 \times 10^9[N/m^2]$. In the all example orthotropic ration is considered to be 0.8.

Example 1

For the first example, we consider an isotropic bar weakened by a straight radial crack. So we set $G = 1$. Firstly, by taking this problem as a bar without any magnetic coating, i.e. $B_0 = 0$ and $R_1 = R_2$, the numerical solution will be compared with existing results to illustrate the efficiency and accuracy of the dislocation method. The center of the radial crack is situated at $r_0 = 0.3R$. The results of dislocation method are compared with the results of the reference [14] in which $k_0 = GMR_1\sqrt{\pi l}/J_0$. The results show negligible difference between the results of the present work and those obtained by [13]. The indexes i and o designate to the inner and outer tips of the crack. We consider a magnetic layer with $R_2 = 1.1R_1$ which the coating is acted as an actuator. The isotropic bar has a radial crack with length $l = 0.4R_1$ wherein the center of the crack is located in the radius of $r_0 = 0.5R_1$. The magnetic induction on the outer radius of the coating layer is set to be B_0. The effect of the magnetic induction (dimensionless form of B_0 or λ) on the stress intensity factor of the crack is shown in Fig. (3).

Table 1 Comparison of calculated results with the results of reference [14] for a straight embedded crack.

l/R	J/J_0		k_{IIIi}/k_0		k_{IIIo}/k_0	
	Present study	Reference [14]	Present study	Reference [14]	Present study	Reference [14]
0.1	0.9982	0.9981	0.2522	0.2518	0.3525	0.3519
0.2	0.9922	0.9922	0.2087	0.2070	0.4113	0.4081
0.3	0.9808	0.9808	0.1695	0.1660	0.4796	0.4703
0.4	0.9612	0.9612	0.1352	0.1295	0.5650	0.5427

We can find that the stress intensity factors subjected to the magnetic effect can be much smaller than that of when the elastic bar is only under torsion. The external loading on the crack surfaces is a function of torsional loading and magnetic induction, therefore by appropriate selection of the magnetic induction, external loading on the crack surfaces can be nearly vanished and stress intensity factors of the crack tips can be vanished. As it can be seen, there is a minimum value for the nondimensional stress intensity factor of each crack tip. This minimum can be reached at different values of λ for each crack tip. Therefore, as a rule of thumb, by minimizing the value of the average dimensionless stress intensity factors of both crack tips, we may reach the relatively less value for the stress intensity factor of each crack tip. We plot the graph of average dimensionless stress intensity factors of both tips versus λ. By choosing $\lambda \approx -0.95$ we arrive at $\frac{k_{IIIi}+k_{IIIo}}{2k_0} \approx 0.16$ which is representative for $\frac{k_{IIIi}}{k_0} \approx 0.16$ and $\frac{k_{IIIo}}{k_0} \approx 0.16$. Generally speaking, the intersection of the graphs of $\frac{k_{IIIL}}{k_0}$ and $\frac{k_{IIIR}}{k_0}$ versus λ in which $k_{IIIL} = k_{IIIR}$ can specifies a suitable value for λ. In this value of λ, the average dimensionless stress intensity factors of both tips are almost minimum.

The stress intensity factors must be decreased by adding the stiffer coating. But for magnetic coating, the elastic shear stiffness constant (C_{44}) is less than that of orthotropic bar (G_{rz}). Therefore, in lack of the magnetic field, increasing the weaker magnetic coating thickness increases the stress intensity factors providing that the outer radius of the coating to be constant. On the other hand, the stress intensity factors are under the influence of both of the magnetic fields and the coating thickness. To illustrate this, by setting $\lambda = 0.01$ or $\lambda = 0.03$, the variations of the stress intensity factor as a function of the relative magnetic coating thickness $(R_2 - R_1)/R_2$ are plotted in Fig. (4). As it can be seen for $\lambda = 0.03$ increasing of the stress intensity factor with enlarging the coating thickness $t = R_2 - R_1$ is more considerable in comparison with $\lambda = 0.01$.

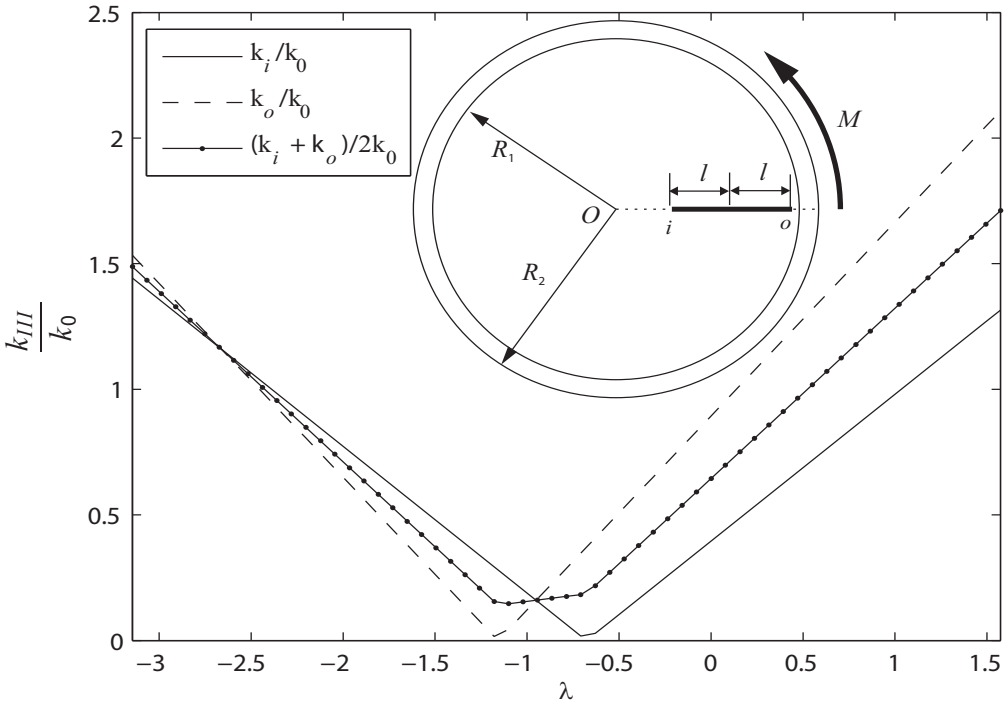

Figure 3 Graph of the dimensionless stress intensity factor versus λ for a straight crack

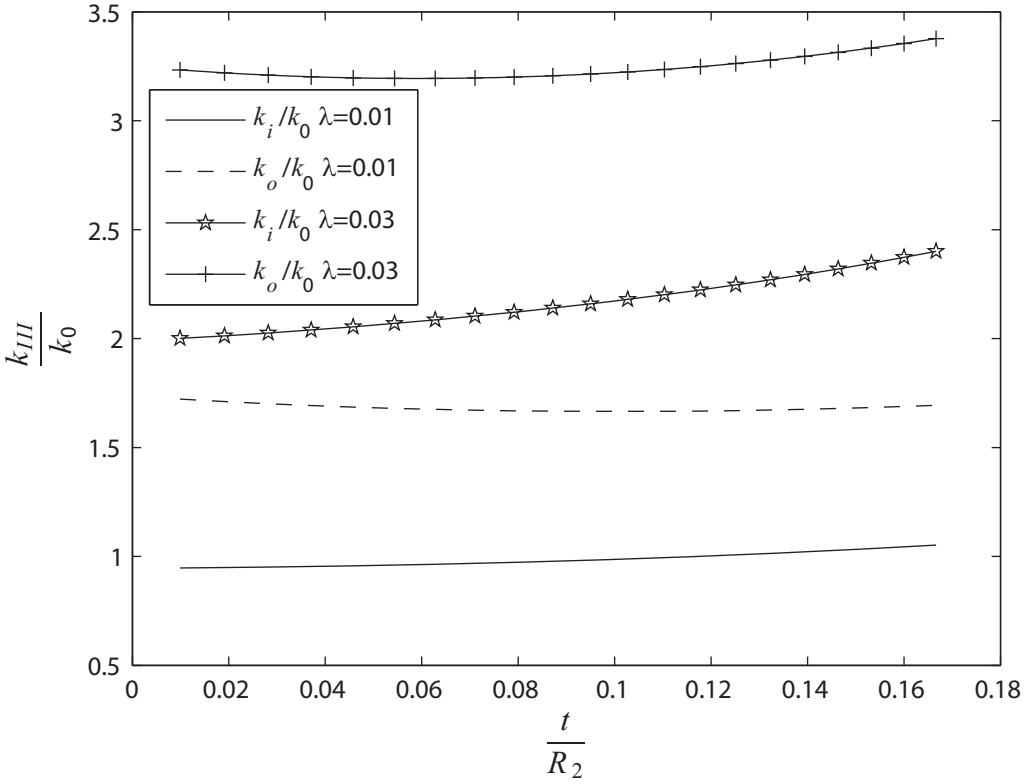

Figure 4 Variation of the normalized stress intensity factor versus the coating thickness for two different values of the λ

Fig. (5) shows the variations of normalized stress intensity factor versus the normalized crack length l/R_1 for each the crack tip. The coating thickness is set to be $t = 0.1R_1$ and the dimensionless magnetic induction is chosen as $\lambda = 0.01$. The stress intensity factor at the outer crack tip increases with the growth of the crack length. But for the inner crack tip, the stress intensity factor slightly decreases initially because of approaching it to the center of the bar wherein the stress components are least. Finally, we absorb that the growth of the crack length is dominant factor in increasing of the stress intensity factor. It is also obvious that torsional rigidity will decrease with the increase of the crack length. In Fig. (6), we illustrate the variation of the normalized torsional rigidity J/J_0 versus the crack length.

Example 2

As the second example, consider the torsional problem of an isotropic bar weakened by an eccentric circular crack with radius $a = 0.5R_1$ as shown in Fig. (7). Because of lack of an example for cracked bar with magnetic coating, we validate the work with a cracked coatless bar under torsion. In this example, the numerical results was compared with the ref [15] by setting $B_0 = 0$ and $R_1 = R_2 = R$. Based on the data shown in Fig. (7) and Fig (8), in which $k_0 = G_{rz}MR_1\sqrt{\theta a}/J_0$, there is a relatively good agreement between the results of the dislocation method and the results reported by Wang and Lu in the ref [15].

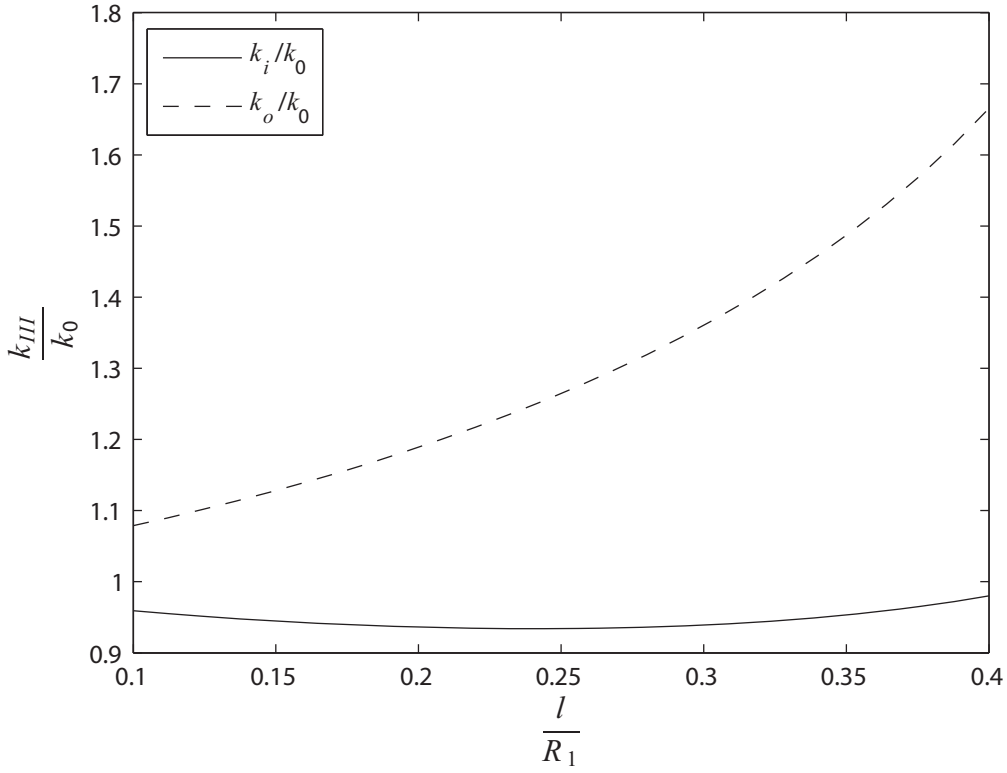

Figure 5 Variation of the normalized stress intensity factor versus the normalized crack length

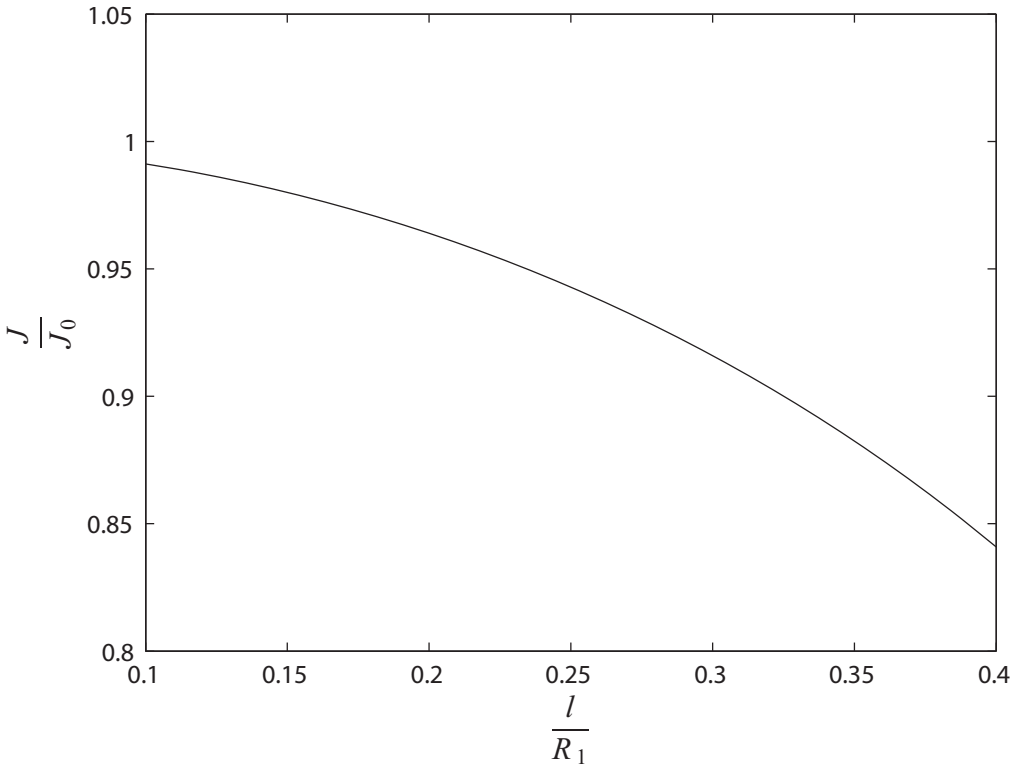

Figure 6 Variation of the normalized torsional rigidity versus the normalized crack length

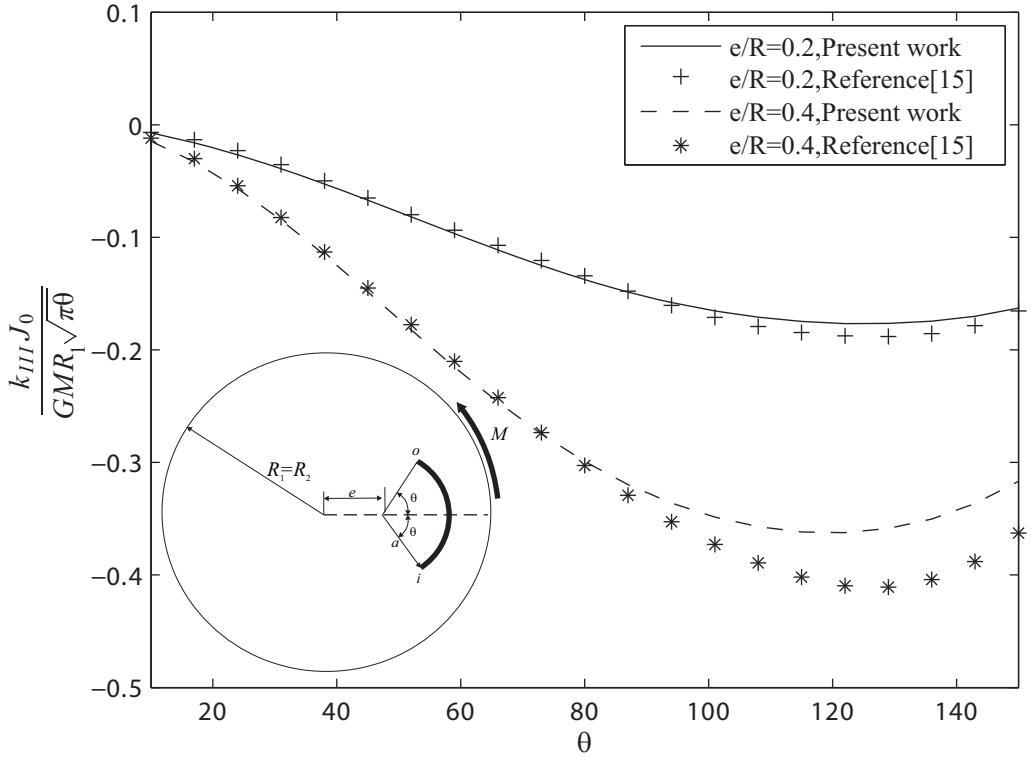

Figure 7 Variation of stress intensity factors with θ for a circular crack

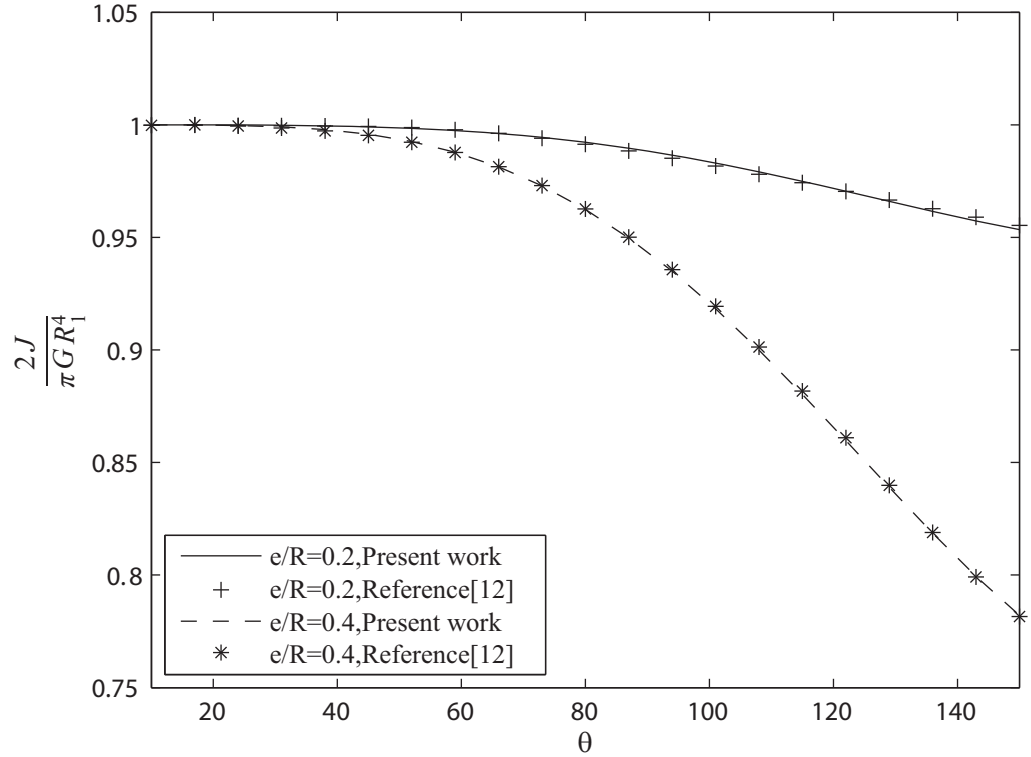

Figure 8 Variation of normalized torsional rigidity with θ for a circular crack

In continuation of this example, we consider an orthotropic bar with the magnetic coating with thickness $0.1R_1$. The circular crack in the orthotropic bar is considered as a quarter of an eccentric circle with radius $a = 0.5R_1$. On Fig. (9) we have represented the dependence of the magnitude of stress intensity factor on λ. In fact, stress intensity factor can be vanished by considering the effect of coating layer. Again, the intersection of the graphs of the stress intensity factors of both crack tips versus λ can specify a good candidate for λ which almost minimizes both the stress intensity factors of the crack tips.

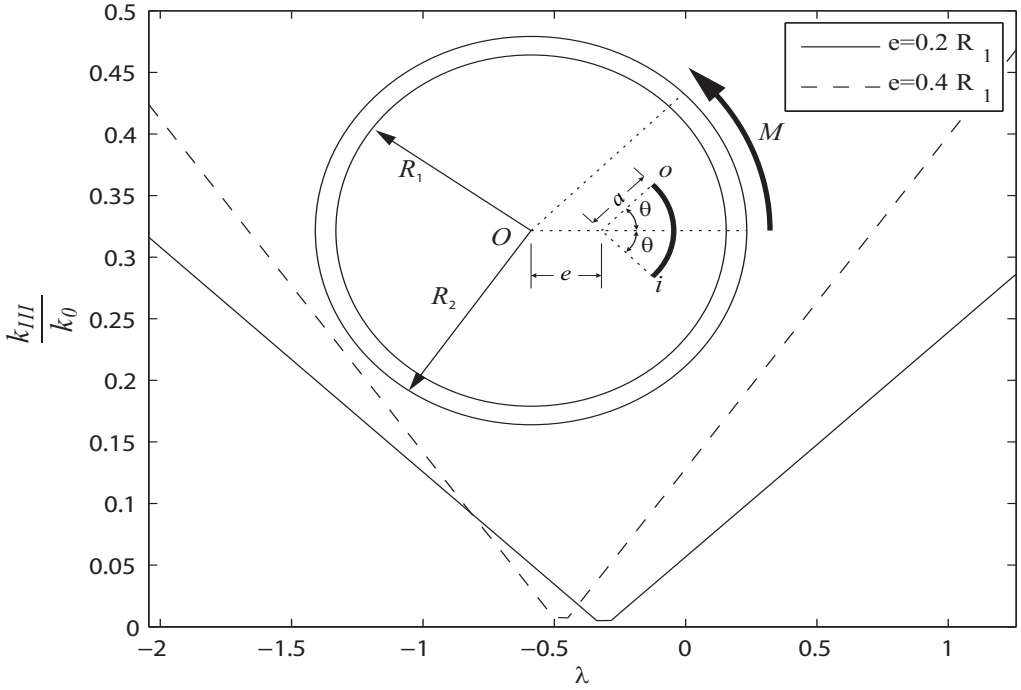

Figure 9 Variation of the stress intensity factors with λ for an eccentric circular crack

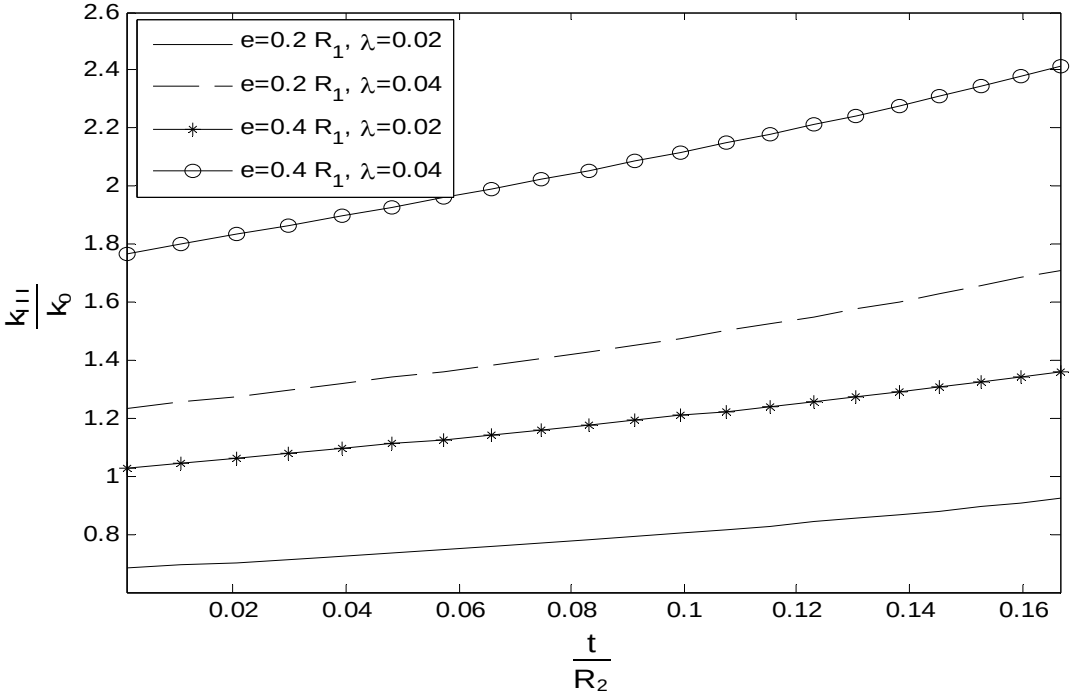

Figure 10 Comparison of the normalized stress intensity factor versus the relative coating thickness for two different values of the λ

The variation of non-dimensional stress intensity factor with relative coating thickness is plotted in Fig. (10). As it can be seen, for different values of λ, the graphs of stress intensity factors versus the relative coating thickness have same trends as the coating thickness is increased. For $\lambda = 0.04$ increasing of the coating thickness magnifies the stress intensity factors of the crack tips more than that of $\lambda = 0.02$. In what follows, the effect of crack length on the stress intensity factor and torsional rigidity for two different crack eccentricities is illustrated in Figs. (11) and (12) respectively. For the crack with small eccentricity, $\lambda = 0.02$ provide the smaller stress intensity factor in comparison with $\lambda = 0.04$. A similar trend as the crack with big eccentricity can be realized. Viewing the Fig. (11), it is known that for $\lambda = 0.02$, the normalized the torsional rigidity will be decreased with growing the crack length.

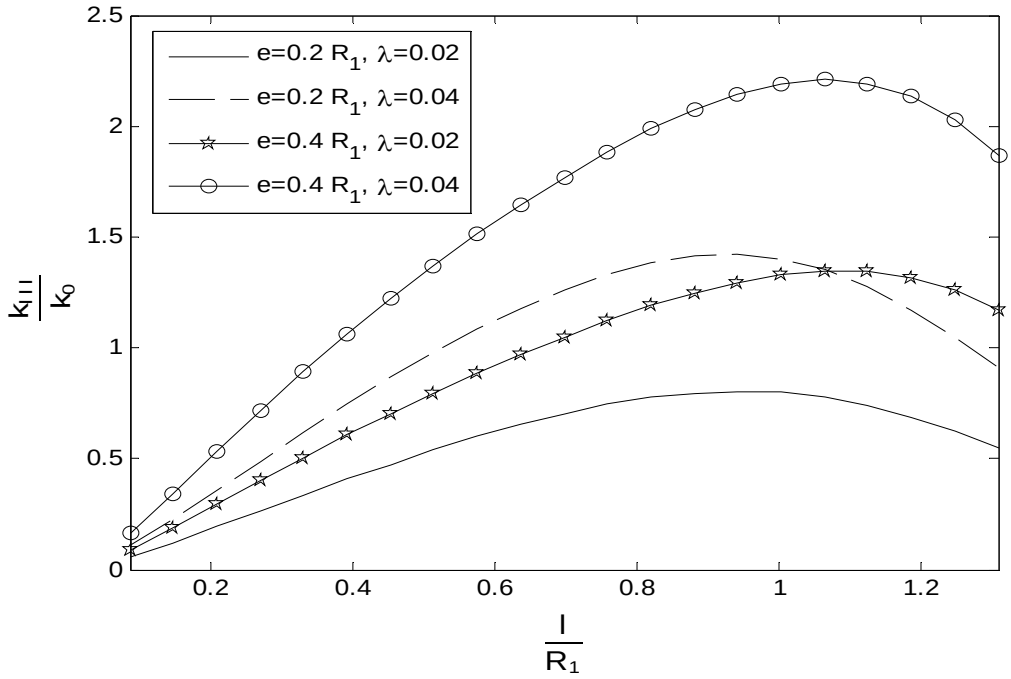

Figure 11 Graphs of the normalized stress intensity factor versus the length of the crack for a circular crack

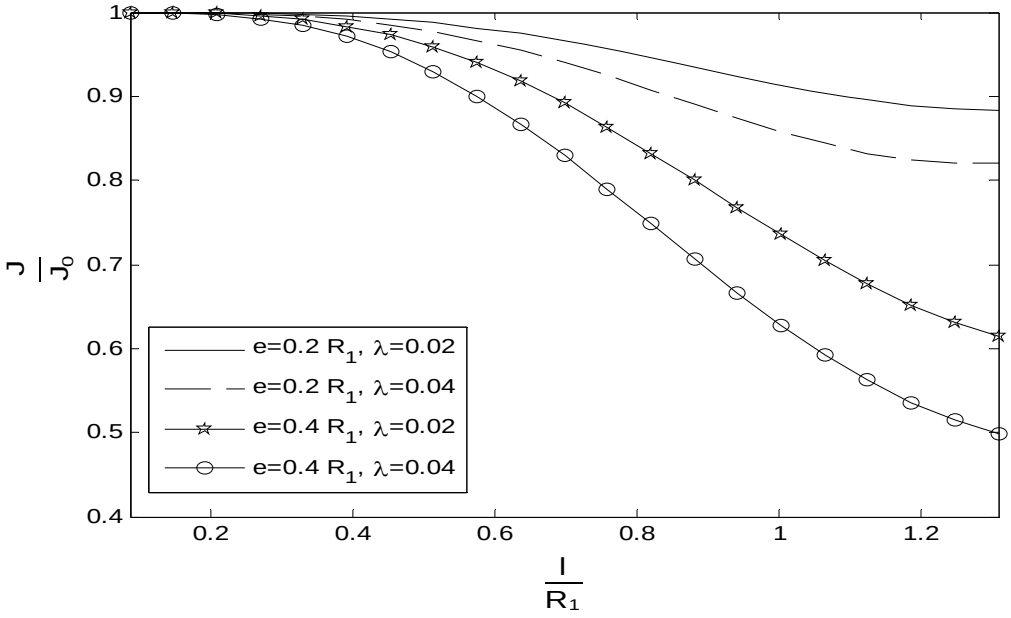

Figure 12 Graphs of the normalized torsional rigidity versus length of the circular crack

Example 3

In the following examples, we consider an orthotropic bar with a magnetic coating weakened by one embedded crack perpendicular to the radial direction as shown in Fig. (13). The crack radial distance is $d = 0.2R_1$ where the crack length $2l = 0.2R_1$ and the layer thickness $0.1R_1$ are constants. Variations of normalized stress intensity factor at the crack tip, k_{III}/k_0 in which $k_0 = G_{rz}MR_1\sqrt{\pi l}/J_0$, as a function of the normalized parameter λ are plotted in Fig. (13). It is obvious that the stress intensity factors can be vanished by setting λ to a suitable value. We recall that the stress intensity factors for both tips are identical because of the symmetry of the problem. In the next graph of this example, by assuming $2l = 0.2R_1$ and $\lambda = 0.4$ or $\lambda = 0.7$, the effect of the relative coating thickness on the stress intensity factor is studied, as shown in Fig. (14). As it can be seen decreasing of λ from 0.7 to 0.4 attenuates the stress intensity factors of the crack tip while the stress intensity factors are increased by enlarging the relative coating thickness.

Figs. (15) and (16) display the variations of the normalized stress intensity factor and torsional rigidity versus the normalized crack length for $\lambda = 0.4$ and $\lambda = 0.7$. The coating thickness is set to be $t = 0.1R_1$. By increasing the dimensionless crack length l/R_1, the crack tips approach to the outer boundary of the bar which corresponds to portions of the bar cross-section with higher levels of the stress field. As one expected, the normalized stress intensity factor of the crack tips should be generally increased by the growth of the crack length. Although by choosing other values of λ, it is possible to decrease the normalized stress intensity factor with enlargement of the crack length. Also the normalized torsional rigidity must be decreased by growing the crack length since this makes the cross-section to be weaker and weaker.

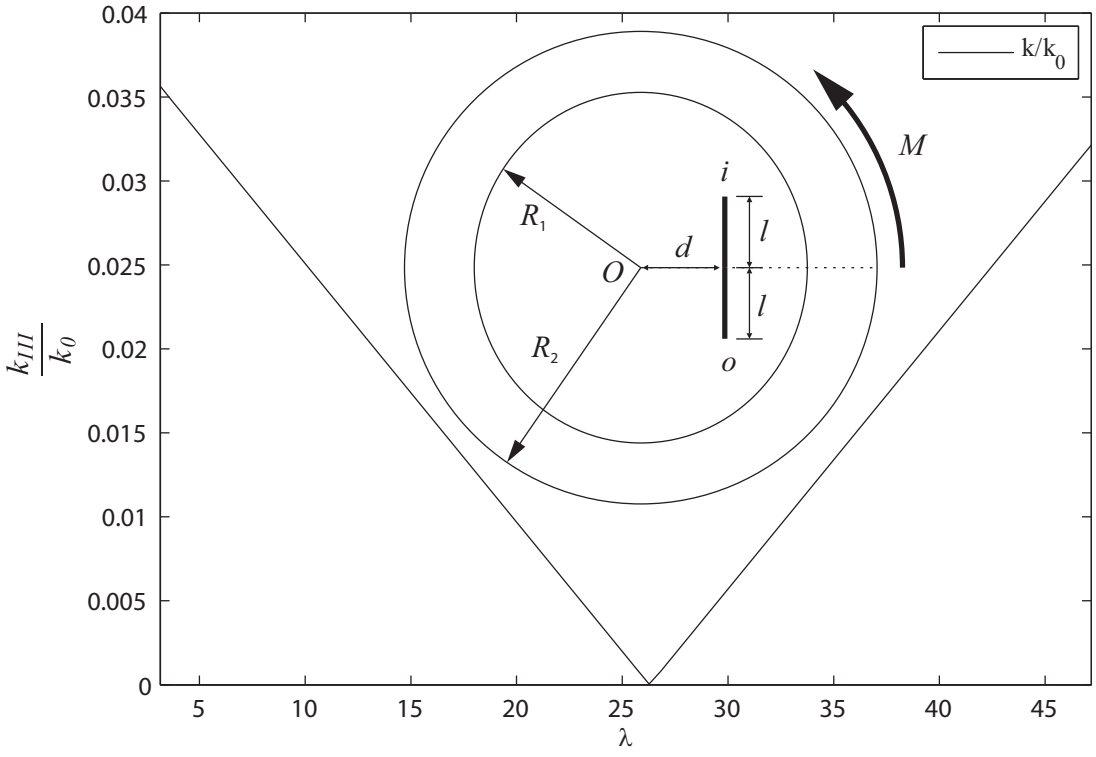

Figure 13 Normalized stress intensity factor as a function of the non-dimensional parameter λ for an embedded crack

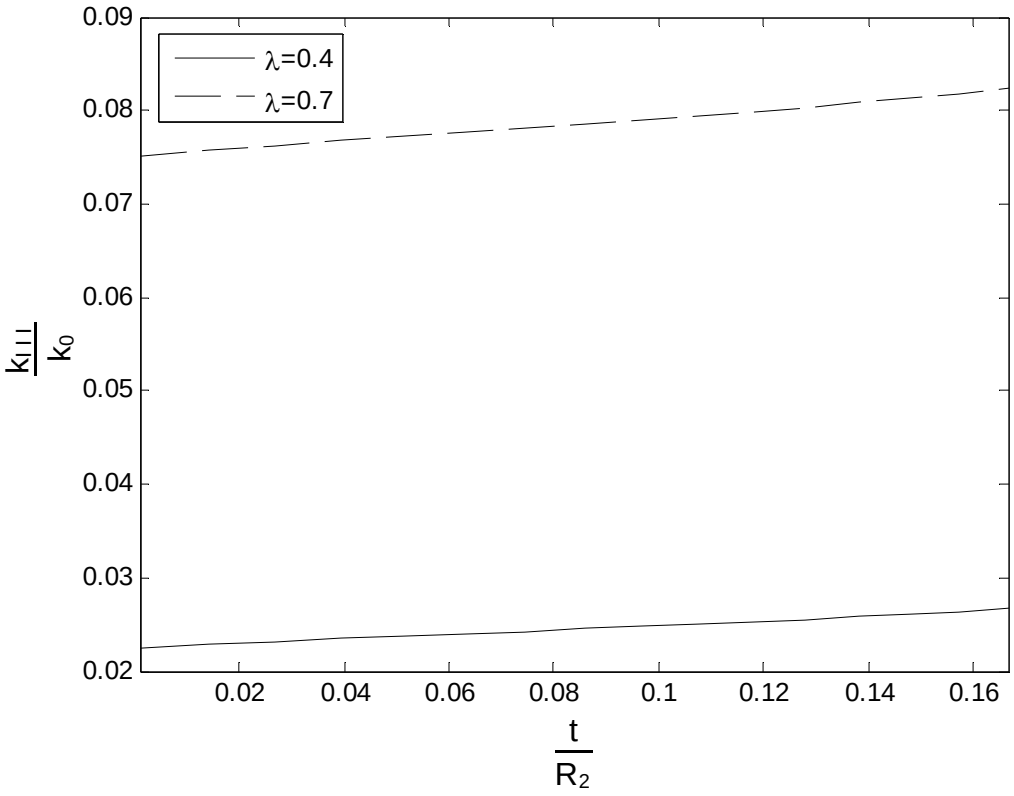

Figure 14 Variation of the normalized stress intensity factor versus coating thickness for an embedded crack

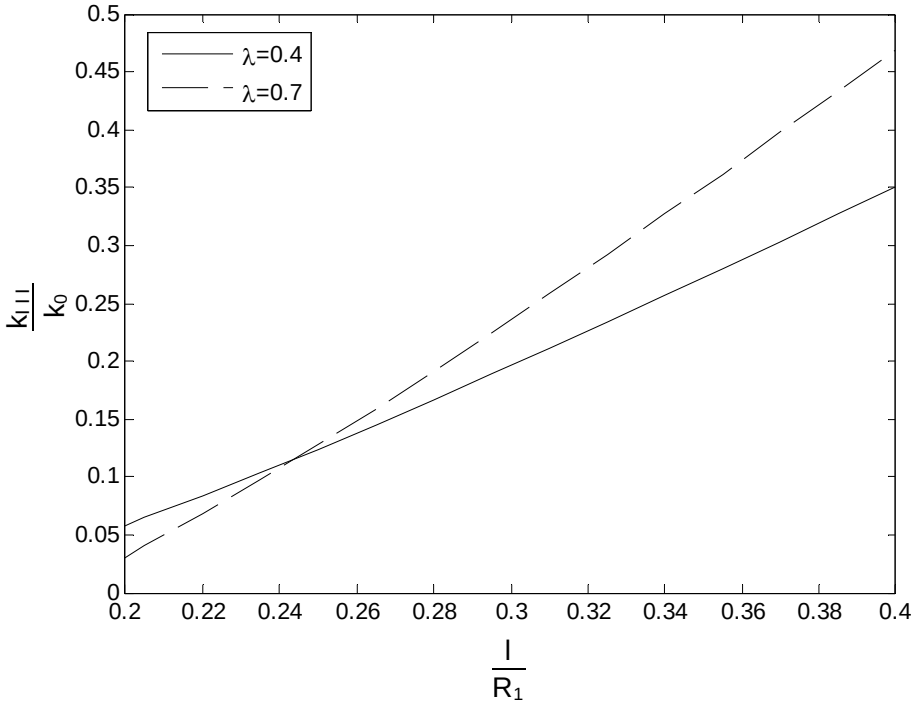

Figure 15 Variation of the normalized stress intensity factor versus length of the crack for an embedded crack

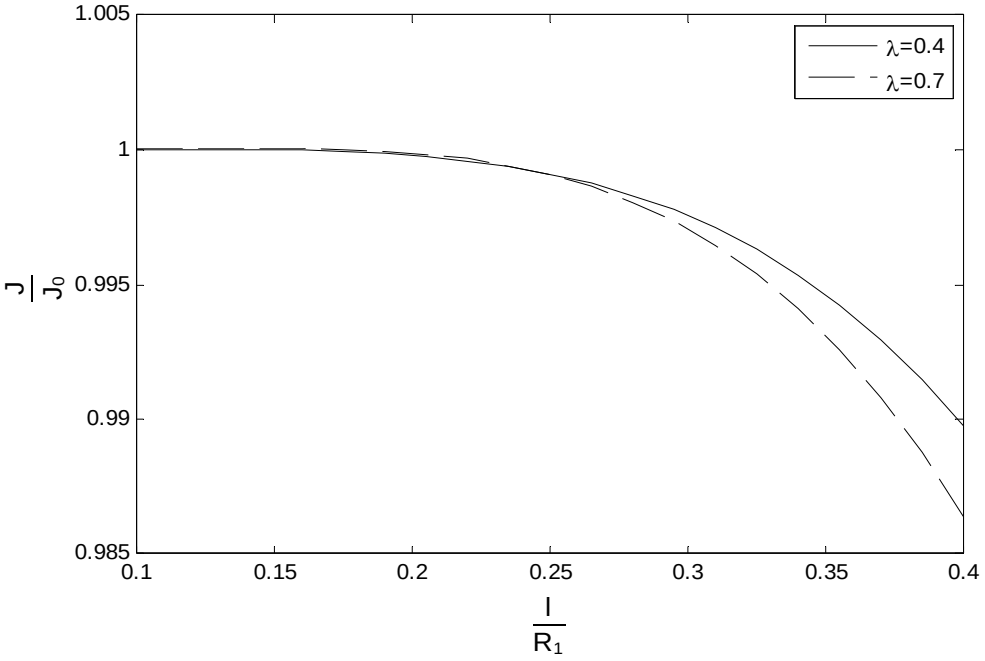

Figure 16 Variation of the normalized torsional rigidity versus length of the crack for an embedded crack

Example 4

In the last example, we analyze the orthotropic bar weakened by two embedded straight cracks with constant length $2l = 0.1R_1$, as shown in Fig. (17). The lengths of the cracks are equal and one tip of the each crack is fixed and located on a circle with radius $a = 0.75R_1$. In other words, each crack is apart the cord with central angle 45 degrees.
The plots of the normalized stress intensity factor as a function of the λ for each of the tips and also the averaged stress intensity factors are illustrated in Fig. (17). For $\lambda \approx 0.75$ the stress intensity factors of the both crack tips are simultaneously the smallest.

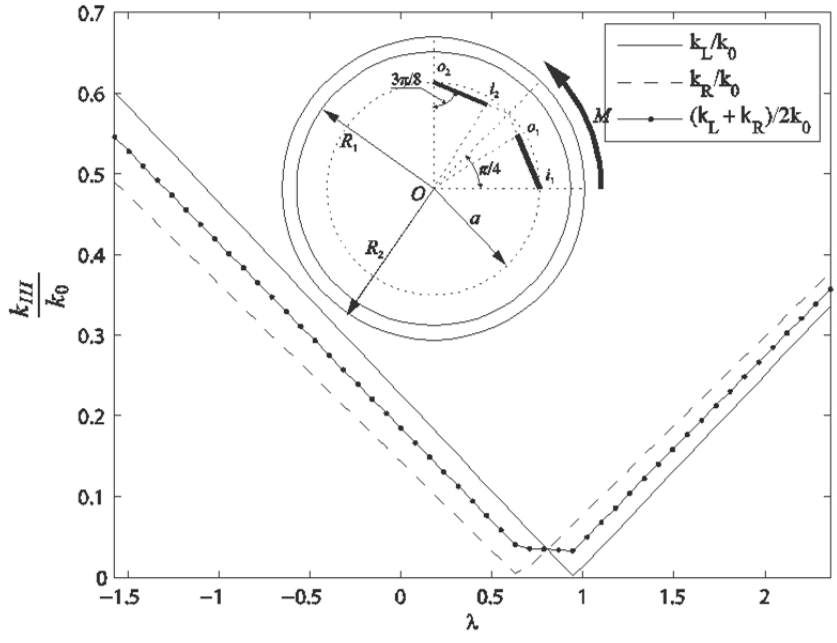

Figure 17 Graphs of the normalized stress intensity factors versus λ for two symmetric cracks

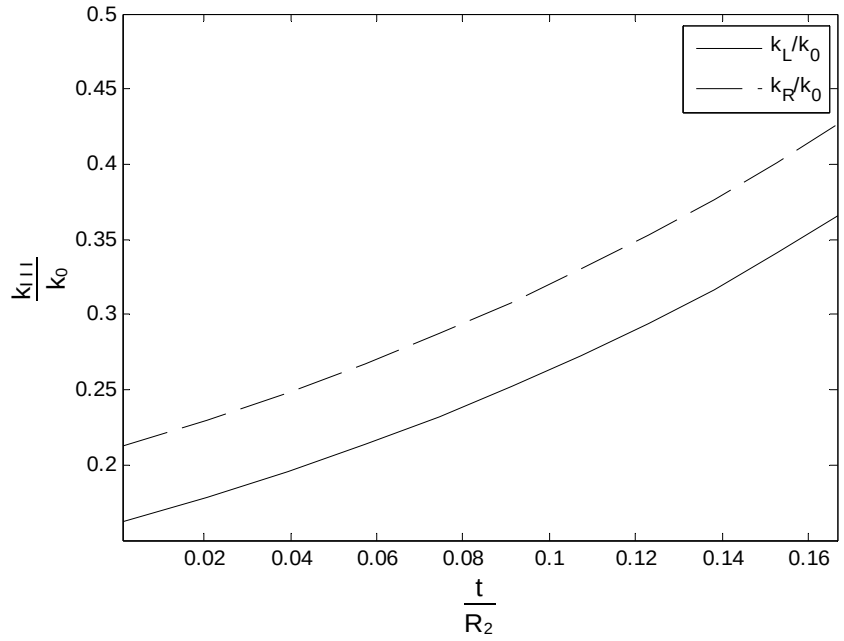

Figure 18 Graphs of the normalized stress intensity factors versus the coating thickness for two symmetric cracks

In the next graph of this section, we can observe the variation of the normalized stress intensity factors versus the relative coating thickness by assuming $\lambda = 0.02$ and $2l = 0.2R_1$ in Fig. (18). As it can be seen, the normalized stress intensity factors are increased by the extension of the coating thickness. In the following, the result of the normalized stress intensity factors and torsional rigidity are depicted in terms of the dimensionless crack length in Fig. (19) and Fig. (20) respectively. The results are evaluated for $\lambda = 0.02$. It can be seen that for each of the crack tips, when the length of the cracks grow, the value of the normalized stress intensity factor approaches a maximum value. Reversely as expected, the computed normalized torsional rigidity is decreased with the crack growth.

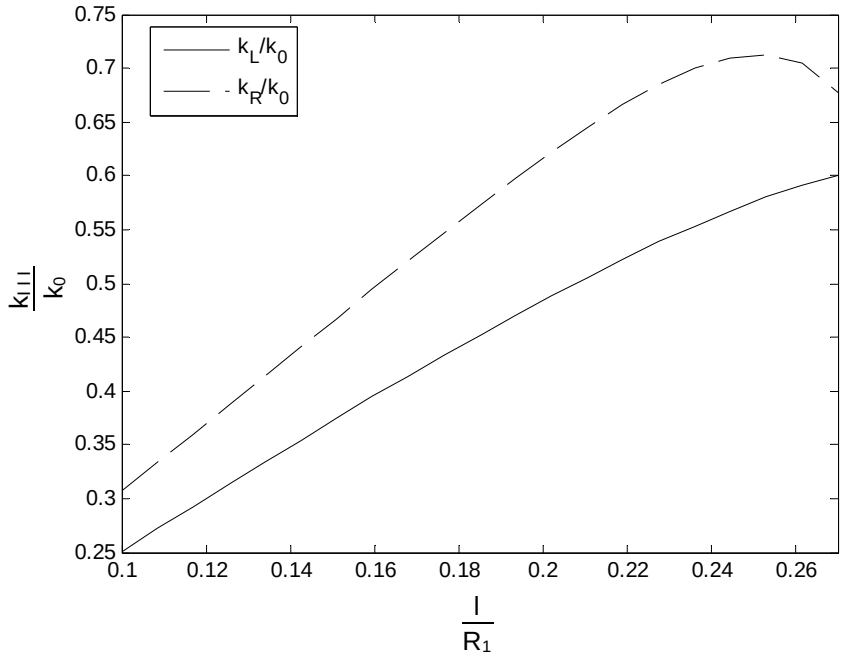

Figure 19 Graphs of the normalized stress intensity factors versus the length of the cracks

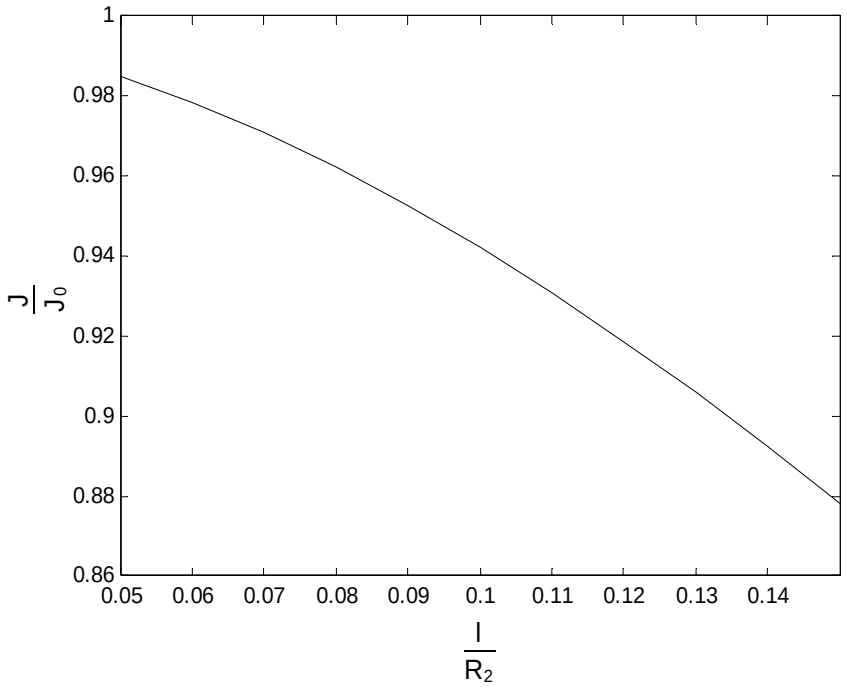

Figure 20 Graphs of the normalized torsional rigidity versus the length of the cracks for two symmetric cracks

5 Conclusion

In the present paper, a torsion problem of an orthotropic bar reinforced by a magnetic layer is studied using the dislocation distributed technique.
Numerical results are also presented and it can be found that:
1. Stress field around the crack tip depends on the magnetic induction on the outer surface of the coating and an appropriate value of the magnetic induction should be determined to minimize the stress intensity factor.
2. Thickness of the coating accompanying with the magnetic induction plays a significant rule in the reduction or magnification of the stress intensity factors.
3. By increasing of the crack length, the stress intensity factors go up and the torsional rigidity deceases.

Acknowledgment

The authors would like to acknowledge Islamic Azad University, Karaj Branch (Iran), for financial support of this research.

References

[1] Ecsedi, I., and Baksa, A., "A Variational Formulation for the Torsional Problem of Piezoelastic Beams", Applied Mathematical Modelling, Vol. 36, pp. 1668-1677, (2012).

[2] Ecsedi, I., and Baksa, A., "Prandtl's Formulation for the Saint–Venant's Torsion of Homogeneous Piezoelectric Beams", International Journal of Solids and Structures,Vol. 47, pp. 3076-3083, (2010).

[3] Talebanpour, A., and Hematiyan, M.R., "Torsional Analysis of Piezoelectric Hollow Bars", International Journal of Applied Mechanics, Vol. 6, pp. 1-18 (2014).

[4] Maleki, M., Naei, M.H., Hosseinian E., and Babahaji, V., "Exact Three-dimensional Analysis for Static Torsion of Piezoelectric Rods", International Journal of Solids and Structures, Vol. 48, pp. 217-226, (2011).

[5] Maleki, M., Naei, M.H., and Hosseinian, E., "Exact Three-dimensional Interface Stress and Electrode-effect Analysis of Multilayer Piezoelectric Transducers under Torsion", International Journal of Solids and Structures, Vol. 49, pp. 2230-2238, (2012).

[6] Zehetner, C., "Compensation of Torsion in Rods by Piezoelectric Actuation", Archive of Applied Mechanics, Vol. 78, pp. 921-933, (2008).

[7] Chen, J.T., Chen, K.H., Yeih, W., and Shieh, N.C., "Dual Boundary Element Analysis for Cracked Bars under Torsion", Engineering Computations, Vol. 15, pp. 732-749, (1998).

[8] Hassani, A., and Faal, R.T., "Saint-Venant Torsion of Orthotropic Bars with a Circular Cross-section Containing Multiple Cracks", Mathematics and Mechanics of Solids, Vol. 21, pp. 1198-1214, (2014).

[9] Chen, J.T., Lee, Y.T., Chou, K.H., and Lee, J.W., "Image Location for Screw Dislocation A New Point of View", Boundary Value Problems, Article ID. 731741, pp. 1-13, (2010).

[10] Chen, J., Chou, K., and Lee, Y., "A Novel Method for Solving the Displacement and Stress Fields of an Infinite Domain with Circular Holes and/or Inclusions Subject to a Screw Dislocation", Acta Mechanica, Vol. 218, pp. 115-132, (2011).

[11] Bixing, Z., Anders, B., and Niklasson, A.J., "Antiplane Shear Waves from a Piezoelectric Strip Actuator: Exact Versus Effective Boundary Condition Solutions", Smart Materials and Structures, Vol. 13, pp. 161-168, (2004).

[12] Faal, R.T., Fotuhi, A.R., Fariborz, S.J., and Daghyani, H.R., "Antiplane Stress Analysis of an Isotropic Wedge with Multiple Cracks", International Journal of Solids and Structures, Vol. 41, pp. 4535-4550, (2004).

[13] Yu-lan, L., Zhi-qing, M., and Ren-ji, T., "The Solution of Integral Equations with Strongly Singular Kernels Applied to the Torsion of Cracked Circular Cylinder", Applied Mathematics and Mechanics (English Edition), Vol. 14, pp. 899-906, (1993).

[14] Fang-ming, T., and Ren-ji, T., "Saint-Venant's Torsion Problem for a Composite Circular Cylinder with Aninternal Edge Crack", Applied Mathematics and Mechanics (English Edition), Vol. 14, pp. 507-516, (1993).

[15] Wang, Y.B., and Lu, Z.Z., "New Boundary Element Method for Torsion Problems of Cylinder with Curvilinear Cracks", Applied Mathematics and Mechanics (English Edition), Vol. 26, pp. 1531-1538, (2005).

Nomenclatures

r	Radial coordinate
R_1	Radius of the isotropic bar
R_2	Outer radius of the isotropic bar
θ	Angular coordinate
α	Angle of twist per unit length
ω	Torsional warping function
ϕ	Magnetic potential function
$\tau_{rz}, \tau_{\theta z}$	Stress component in the radial and angular directions
$G_{rz}, G_{\theta z}$	Shear modulus in the radial and angular directions of the bar
$H(.)$	Heaviside step function
b_z	Dislocation density
$\bar{\omega}(.,.)$	Finite Fourier sine transform of torsional warping function
C_{44}	Elastic shear stiffness constant of the magnetic coating
h_{15}	Piezomagnetic coefficient
γ_{11}	Magnetic permeability
H_r, H_θ	Magnetic fields in the radial and angular directions
B_0	Magnetic induction
J	Torsional rigidity
M	Applied torque
$k(.,.)$	Kernel of integral equation
k_{III}	Stress intensity factor

Appndix A:

$$A_{3n} = R_2^{-n}\Gamma_n\{\frac{b_z}{2n\alpha}C_{eq}(1-\rho_n)\kappa_n + \frac{1-(-1)^n}{n^2\alpha}\frac{e_{15}C_{eq}}{G\varepsilon_{11}}[(1+C_{eq})B_0R_2]\} \quad (A1)$$

$$B_{3n} = R_1{}^n\Gamma_n\{\frac{b_z}{2n\alpha}C_{eq}(1-\rho_n) + \frac{1-(-1)^n}{n^2\alpha}\frac{e_{15}C_{eq}}{G\varepsilon_{11}}[(1-C_{eq})B_0R_2\kappa_n]\}$$

$$C_n = R_2{}^{-n}\{\frac{e_{15}}{\varepsilon_{11}}\Gamma_n\{\frac{1-(-1)^n}{n^2\alpha}\frac{e_{15}C_{eq}}{G\varepsilon_{11}}[(1+C_{eq})B_0R_2] + \frac{b_z}{2n\alpha}C_{eq}(1-\rho_n)\kappa_n\} + (-B_0R_2)\frac{1-(-1)^n}{n^2\alpha\varepsilon_{11}(1-\kappa_n^2)}\}$$

$$D_n = R_1{}^n\{\frac{h_{15}}{\gamma_{11}}\Gamma_n\{\frac{1-(-1)^n}{n^2\alpha}\frac{e_{15}C_{eq}}{G\varepsilon_{11}}[(1-C_{eq})B_0R_2\kappa_n] + \frac{b_z}{2n\alpha}C_{eq}(1-\rho_n) + (-B_0R_2\kappa_n)\frac{1-(-1)^n}{n^2\alpha\varepsilon_{11}(1-\kappa_n^2)}\}$$

Appendix B:

Kernels of the integral equations are:

$$k_{ij}(s,t) = G_{\theta z}\sqrt{(r_j')^2 + \left(r_j\theta_j'\right)^2}\{\frac{G}{2J_0}\left(R_1^2\text{-}r_j^2\right)r_i\cos\varphi_i \tag{B1}$$

$$+\frac{1}{4\pi r_i}\frac{1}{C_{eq}+1}\{\sum_{m=0}^{\infty}\eta^m[2(F_m(\frac{r_i}{R_1},\theta_i\text{-}\theta_j)\text{-}F_m(\frac{R_1 r_i}{R_2^2},\theta_i\text{-}\theta_j))$$

$$+\left(C_{eq}\text{-}1\right)(F_m(\frac{r_i r_j}{R_1^2},\theta_i\text{-}\theta_j)\text{-}F_m(\frac{R_1^2 r_i}{R_2^2 r_j},\theta_i\text{-}\theta_j)) + (1+C_{eq})(F_m(\frac{r_i r_j}{R_2^2},\theta_i\text{-}\theta_j)$$

$$\text{-}F_m(\frac{r_i}{r_j},\theta_i\text{-}\theta_j))]\cos\varphi_i\text{-}\sum_{m=0}^{\infty}\eta^m[2(E_m(\frac{R_1 r_i}{R_2^2},\theta_i\text{-}\theta_j)$$

$$\text{-}E_m(\frac{r_i}{R_1},\theta_i\text{-}\theta_j)) + \left(C_{eq}\text{-}1\right)(E_m(\frac{R_1^2 r_i}{R_2^2 r_j},\theta_i\text{-}\theta_j)\text{-}E_m(\frac{r_i r_j}{R_1^2},\theta_i\text{-}\theta_j))$$

$$+(1+C_{eq})(E_m(\frac{r_i}{r_j},\theta_i\text{-}\theta_j)\text{-}E_m(\frac{r_i r_j}{R_2^2},\theta_i\text{-}\theta_j))]\sin\varphi_i\}\},0 \le r_i \le r_j$$

$$k_{ij}(s,t) = G\sqrt{(r_j')^2 + \left(r_j\theta_j'\right)^2}\{\frac{G}{2J_0}\left(R_1^2\text{-}r_j^2\right)r_i\cos\varphi_i$$

$$+\frac{1}{4\pi r_i}\frac{1}{C_{eq}+1}\{\left(C_{eq}+1\right)[F_0(\frac{r_j}{r_i},\theta_i\text{-}\theta_j)\cos\varphi_i\text{-}E_0(\frac{r_j}{r_i},\theta_i\text{-}\theta_j)\sin\varphi_i]$$

$$\text{-}\sum_{m=0}^{\infty}\eta^m\,[2F_m(\frac{R_1 r_i}{R_2^2},\theta_i\text{-}\theta_j)\text{-}2F_m(\frac{r_i}{R_1},\theta_i\text{-}\theta_j)$$

$$\text{-}(C_{eq}\text{-}1)F_m(\frac{r_j r_i}{R_1^2},\theta_i\text{-}\theta_j)\text{-}(C_{eq}+1)F_m(\frac{r_j r_i}{R_2^2},\theta_i\text{-}\theta_j)]\cos\varphi_i$$

$$+\sum_{m=0}^{\infty}\eta^m\,[2E_m(\frac{r_i}{R_1},\theta_i\text{-}\theta_j) + (C_{eq}\text{-}1)E_m(\frac{r_j r_i}{R_1^2},\theta_i\text{-}\theta_j)$$

$$\text{-}2E_m(\frac{R_1 r_i}{R_2^2},\theta_i\text{-}\theta_j) + (C_{eq}+1)E_m(\frac{r_j r_i}{R_2^2},\theta_i\text{-}\theta_j)]\sin\varphi_i\}\ ,\ \ r_j \le r_i \le R_1$$

The left side of the integral equation (33) is

$$Q_i(s) = \text{-}\frac{2h_{15}C_{eq}}{\pi r_i\gamma_{11}\left(C_{eq}+1\right)}\sum_{j=1}^{N}\int_{-1}^{1}[\Phi(r_i,\theta_i\text{-}\theta_j)\cos\varphi_i\text{-}\Psi(r_i,\theta_i\text{-}\theta_j)\sin\varphi_i]\,dt \tag{B2}$$

$$\text{-}\frac{G_{\theta z}M}{J_0}r_i\cos\varphi_i$$

where all the parameters with index i are functions of s and those with index j are functions of t.